Al-Khwarizmi Engineering Journal, Vol. 10, No. 3, P.P. 25- 38 (2014)

Al-Khwarizmi Engineering Journal

An Experimental Study of the Effect of Vortex Shedding on Solar Collector Performance

Alaulddin Abdulqader Kadim
Department of Engineering Affair/ University of Baghdad
Email:aldina81@yahoo.com

(Received 24 March 2014; accepted 13 July 2014)

Abstract

In this work, the effect of vortex shedding on the solar collector performance of the parabolic trough solar collector (PTSC) was estimated experimentally. The effect of structure oscillations due to wind vortex shedding on solar collector performance degradation was estimated. The performance of PTSC is evaluated by using the useful heat gain and the thermal instantaneous efficiency. Experimental work to simulate the vortex shedding excitation was done. The useful heat gain and the thermal efficiency of the parabolic trough collector were calculated from experimental measurements with and without vortex loading. The prototype of the collector was fabricated for this purpose. The effect of vortex shedding at different operation conditions was examined. The variation of angles of attack and wind velocity leads to different values of vortex loading coefficients and shedding frequencies. The relation between the dynamic characteristics and solar collector performance was evaluated. The finite element method was used to estimate the dynamic characteristic of the solar collector in addition to experimental work to evaluate the relation between the dynamic behavior of the collector and its performance.

Keywords: *Vortex shedding, solar collector efficiency, useful heat gain.*

1. Introduction

In order to deliver high temperatures with good efficiency, a high performance solar collector is required. Systems with light structures and low cost technology for process heat applications up to 400˚C could be obtained with parabolic through solar collectors (PTSC). PTSC can effectively produce heat at temperatures between 50 and 400 ˚C [1]. Most of the solar power plants installed with parabolic collectors are on flat terrain and they may be subjected to some environmental problems. One of problems for large parabolic collector is their stability to track the sun with respect to time very accurately. Any small off tracking as well as the collector structure stability will be affected by strong wind blowing for the regions where the wind velocity is high [2]. Wind loading excites the structures to vibrate with specific deformation pattern called wind-induced vibration. This excitation induced due to many flow phenomenons such as vortex shedding, flutter, buffeting and fluid- structure interaction [3]. This flow phenomenon can affect the performance of solar collector significantly [4]. Holmes et al. [5] studied flow pattern around a microwave dish. They studied wind drag forces on microwave dish antennas and their supporting lattice tower for different angles of attack. They found that, drag coefficient for an isolated dish is maximum with direction normal to the plane of the dish, but does not change in an angular window within 30˚ to the normal of the dish. Raddu and Axinte [6] studied the wind effect on solar flat-plate collectors. They found that when the wind direction is normal to the plate the drag coefficient is maximum. Chevalien and Norton [7] studied rows of solar panels on a model building in a wind tunnel and their sheltering effects. they founded that the number of rows and presence of

sheltering lead to significant decreasing in wind loading. Kopp and Surry [8] performed an experimental research on the total system torque measured at the main drive gear box used for panel's solar tracking system.

In this work, the effect of vortex shedding on collector performance was investigated experimentally. The experimental vortex shedding excitation was determined according to hybrid model and applied to the parabolic trough with specific magnitudes and frequencies. Different values of vortex excitation magnitude and vortex excitation frequency are examined. Then, the collection efficiency of parabolic trough solar collector was measured experimentally first without presence of vortex excitation and second with presence of vortex excitation. Different angles of attack of wind and wind velocities are investigated. The tests were done by using special test rig fabricated for this purpose. The experimental tests have been carried out in Baghdad (AL-Jaderiah) with climatic conditions (latitude of 33.3˚ N, longitude of 44.4˚ E and a standard time meridian of 45˚) during selected days of the months of August, September and October.

2. Vortex Shedding Model

For a bluff body in uniform cross flow, the wake behind the body is not regular but contains distinct vortices. The vortices are shed alternately from each side of the body in a regular manner and give rise to an alternating force on the body. Experimental studies have shown that the frequency, in Hertz, of the alternating lift force is expressed as [9]:

$$f_s = \frac{S\,U}{D} \qquad \text{... (1)}$$

where S: The dimensionless number called the Strouhal number,
U: wind velocity (m/s)
D: is the width of the object perpendicular to the flow (m)

The Strouhal number is determined only by experimental work. For solar collector, it depends on angle of attack of wind (θ). The angles of attack examined in current study are (30˚, 45˚, 60˚, 75˚, 90˚). These angles of attack are shown in figure (1). The values of Strouhal versus these angles of attack are shown in table (1) [10]. The oscillating lift force imposed on a structure of length L and width D, in a uniform cross flow of velocity U, due to vortex shedding is given by [11]:

$$F = \frac{1}{2}\,\rho U^2\, C_L\, DL \sin(2\pi f_s t) = F_o \sin(2\pi f_s t) \qquad \text{... (2)}$$

where

$$F_o = \frac{1}{2}\,\rho U^2\, C_L\, DL$$

t: time (s)

The lift coefficient of solar collector is also depends on the angle of attack. The lift coefficient determined only by experimental work. The values of lift coefficient corresponding to the angles of attack are obtained by using boundary layer wind tunnel tests for the solar collector with specification shown in figure (2) [12]. These values are listed in table (2) [12]. The validity of boundary-layer wind tunnel testing for wind loads on structures is based on similarity arguments and on model-to-full-scale test comparison [12]. In current work, 1/4 model- to-full- scale was used and the specification of prototype shown in Figure (2).

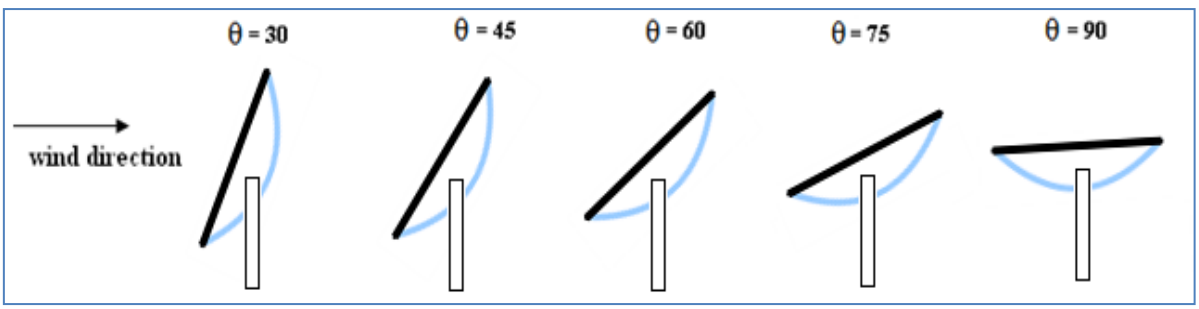

Fig. 1. The angles of attack.

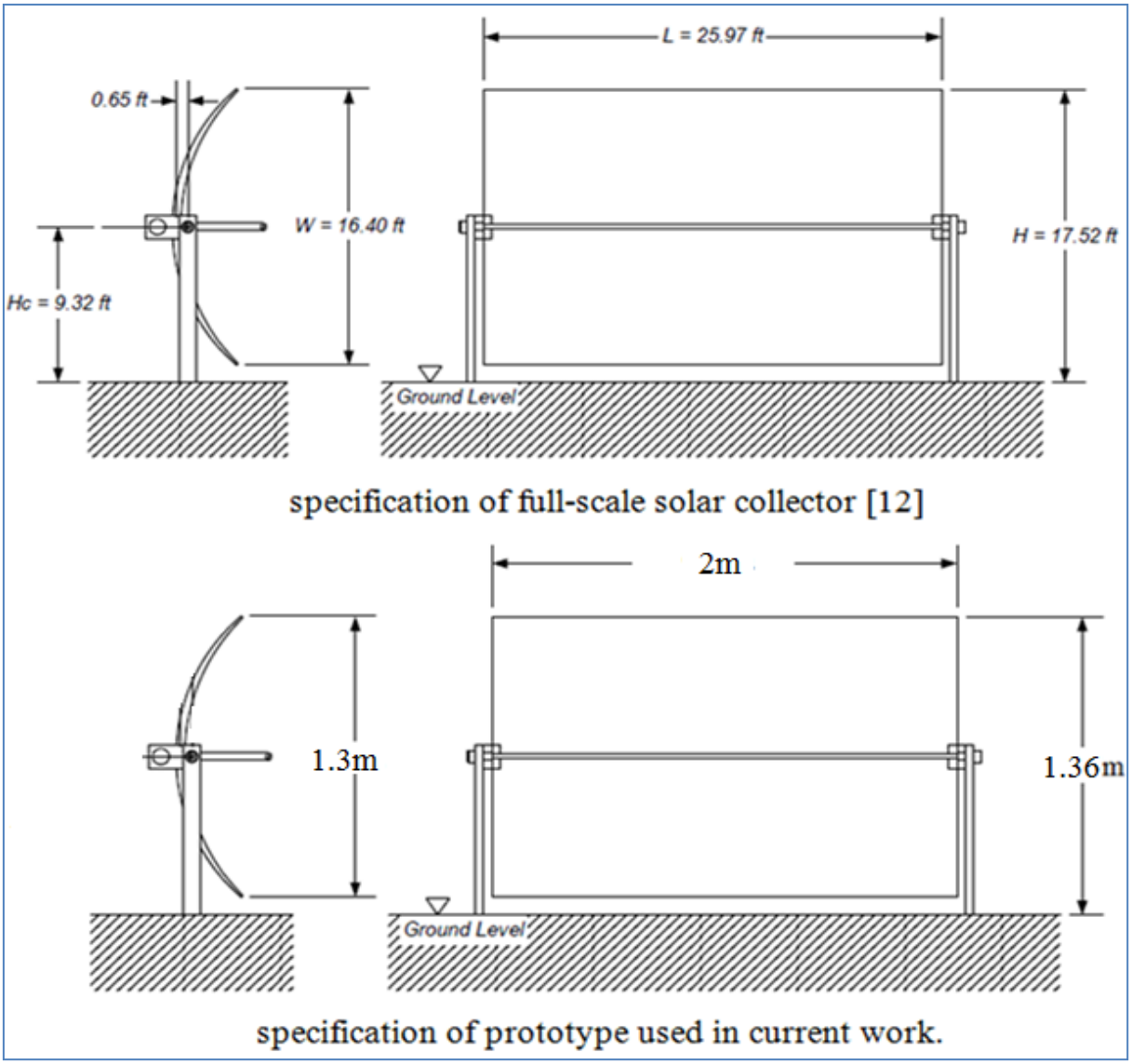

Fig. 2. Specification of full scale solar collector and prototype used in current work.

Table 1,
Strouhal number versus the angle of attack [10].

θ	30˚	45˚	60˚	75˚	90˚
S	0.23	0.216	0.201	0.196	0.182

Table 2,
Lift coefficient versus the angle of attack [12].

θ	30˚	45˚	60˚	75˚	90˚
C_L	1.1	1.5	1.9	0.9	0.2

The oscillating lift force imposed on a parabolic trough can be computed for each angle of attack and wind velocity.

3. Experimental Representation of Vortex Shedding Excitation

The oscillating force due to vortex shedding can be simulated experimentally. The magnitude and frequency are calculated from equations 1 and 2. The experimental apparatus used to simulate the oscillating force is consist of:

1. Function generator used supply wave signal with specific type, amplitude, and frequency
2. Power amplifier used to amplify the signal which come from function generator.
3. Electro-mechanical shaker used to supply excitation force to the structure.
4. Nylon stinger connects the electro-mechanical shaker to the structure.

The apparatus can be used to supply oscillating force (harmonic or repeated) in specific magnitude and frequency. Figure 3 shows the schematic diagram of the system of application of oscillating force.

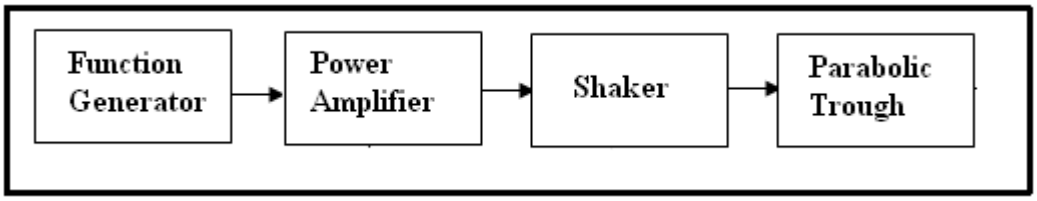

Fig. 3. Schematic diagram of oscillating force supply system.

4. Solar Collector Setup

The prototypes used in this study are fabricated by using special mold. A special composite material [polyester resin+ E-glass fiber] was applied to obtain the final product of parabolic trough solar collector. Before applying the polyester and E-glass fiber layers, a layer of resin which called (gel coat) is applied. This layer will make the interior surface of trough very smooth. Fine brushing was applied on the mixture of polyester resin and E-glass fiber (chopped fiber) to ensure isotropic properties for the material. Then the interior surface coated by reflective material (mirror film) as shown in Figure (4).

Fig. 4. The parabolic trough with reflective material and support frame.

5. Solar Radiation Absorption and measuring System

The first component of solar radiation absorption system is the reflective surface which was obtained by using reflective mirrors film as in Figure (4) which has been introduced to concentrate solar technology as an alternative to mirrored glass reflectors. The second component is the copper pipe which is placed parallel to the rotation axis along the focal line. The wall thickness of the pipe is small (less than 0.5mm) to ensure quick transfer of energy from solar radiation to the working fluid which flow inside the pipe. Black paint is used to cover the outside surface of the pipe to increase the absorbance of the incident solar irradiance and reduces the reflectance. The interior diameter of the pipe is (12 mm). Pump of (0.1 kg/s) flow rate is used for circulating the water through a closed circuit consist of the absorbance pipe, flexible tube, connections and insulating storage tank. The water temperatures at inlet (T_i) and outlet (T_o) of the absorber tube, water mean flow rate (m_w), ambient temperature (T_{amb}) and solar radiation intensity (q_s) are measured using two calibrated K-type thermocouples probes. The solar radiation intensity was measured by using a pyranometer. The schematic diagram of the experimental apparatus is shown in picture (5).

The useful heat can be defined on the base of fluid difference temperature as [13]

$$Q = m_w . C_w . (T_e - T_i) \quad \ldots (3)$$

and the solar collector efficiency is:

$$\eta_c = \left[\frac{m_w . C_w . (T_e - T_i)}{q_s . A}\right] \quad \ldots (4)$$

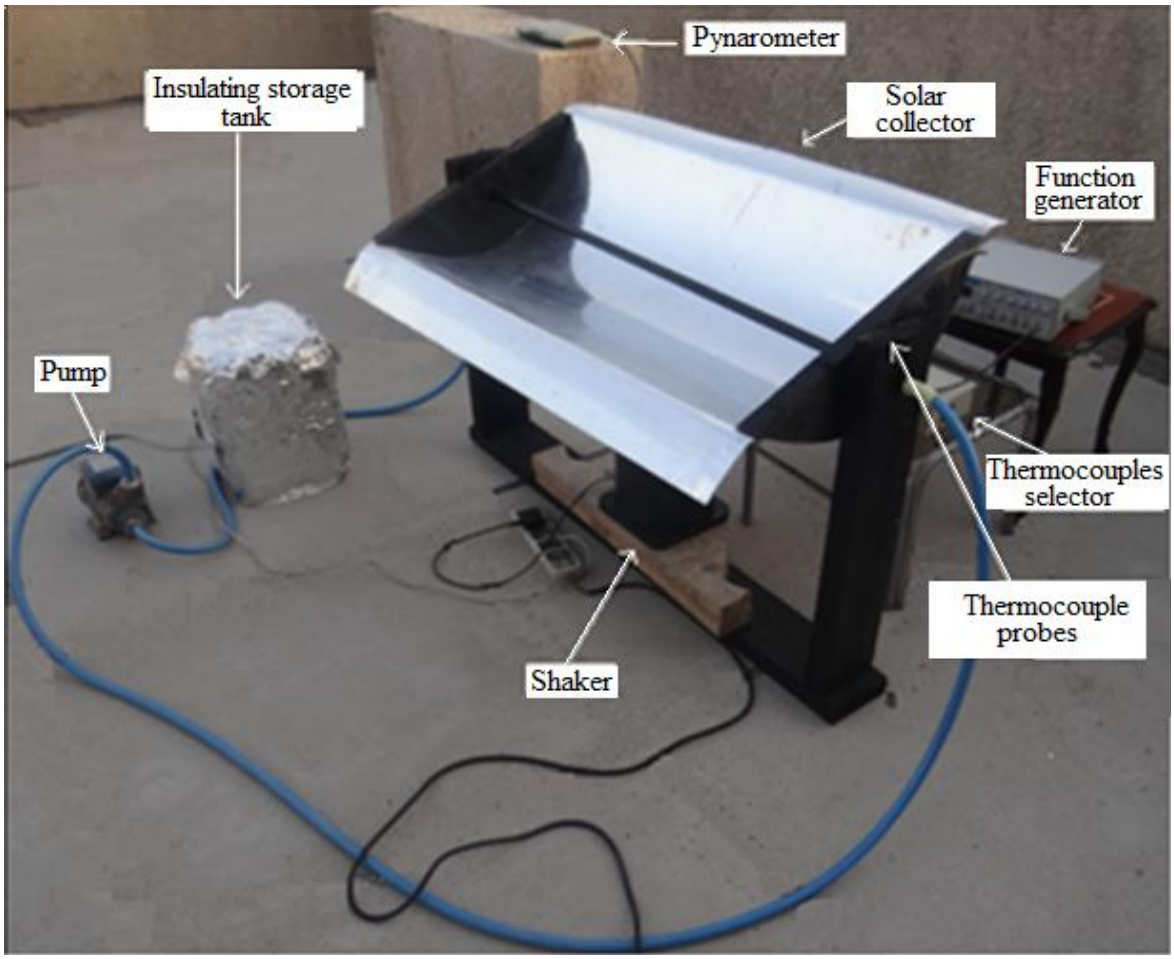

Fig. 5. The test rig.

6. Natural Frequencies and Deflection Measuring System

Natural frequencies was measured by using experimental modal analysis technique. the system of measuring included the excitation part and the response measuring part. The excitation part as previous included function generator, amplifier, electromechanical shaker, and nylon stinger. The response measuring system included piezoelectric accelerometer, charge amplifier and digital storage oscilloscope. The experimental results of natural frequencies are obtained by changing the excitation frequency and recording the behavior of the response of the structure to the changing of excitation frequency until the response of the structure reach to one of the peak values. The value of excitation frequency corresponding to one peak response equal to one value of natural frequencies. The response (deflection) of structure to dynamic excitation are also measured and recorded by using piezoelectric accelerometer, charge amplifier, and digital storage oscilloscope.

7. Numerical Simulation

The numerical simulation was used in current study to perform two types of analysis which are:
1- Modal analysis to estimate the natural frequencies for the structure. The estimation of natural frequencies was done to avoid applying excitation frequency close to any of these natural frequencies. Applying excitation frequencies close to any natural frequency will lead to undesired response for the structure.
2- Harmonic analysis to estimate the response of the structure to harmonic excitation which will apply to structure to simulate the wind loading due to vortex shedding.

The numerical simulation was done by using software package (ANSYS Mechanical APDL). Simulation parameters such as model geometry, boundary conditions, material properties, element type, and governing equation solution scheme are chosen carefully to give the optimum results of natural frequencies and the response to harmonic excitation. The numerical results of natural frequencies were verified with corresponding

experimental results. . The detailed information about simulation parameters and the figures of element type and meshing model are shown in appendix 1.

8. Results and Discussion

First, the first five natural frequencies are estimated numerically and experimentally. Table 3 lists the value of the first five natural frequencies.

Table 3,
First five natural frequencies.

Natural frequency	Numerical(Hz)	Experimental(Hz)	Error percentage
First	54	49	9.26 %
Second	63	61	3.17%
Third	78	71	8.97%
Fourth	94	88	6.383%
Fifth	112	103	8.03%

The deformation of parabolic trough solar collector due to vortex shedding excitation will be introduced. The magnitude and frequency of vortex shedding excitation are computed and listed in table (4) for each angle of attack and wind velocity. The deflection of the parabolic trough is evaluated numerically and experimentally. Figure (6 and 7) shows the deflection of the trough at each wind velocity and angle of attack. It is clear from these results that both angle of attack and wind velocity have an effect on deflection pattern of trough but the effect of velocity is larger than the effect of angle of attack. This estimation established because the difference in deflection pattern when the angle of attack is constant and wind velocity changed is larger than the difference in deflection when the velocity was constant and angle of attack changed.

Table 4,
Magnitude and frequency of wind excitation force.

θ = 30°	**Velocity (m/s)**	**fs (Hz)**	**Fo (N)**
	5	0.75	4.175
	10	1.5	33.287
	15	2.24	92.688
θ = 45°			
	5	0.7	5.314
	10	1.4	42.4
	15	2.1	142.366
θ = 60°			
	5	0.652	6
	10	1.3	49.88
	15	1.96	168.5
θ = 75°			
	5	0.636	2.897
	10	1.272	23.12
	15	1.9	77.4
θ = 90°			
	5	0.59	0.59
	10	1.18	4.76
	15	1.772	16

Figure (8) shows the maximum value of deflection of trough versus the angles of attack and wind velocity. It is observed that the deflection of trough has maximum value at angle of attack ($\theta = 60^{\circ}$) and minimum value at angle of attack ($\theta = 90^{\circ}$). This observation was recorded for all wind velocity. Also, the value of deflection increases when wind velocity increases. This result is normal because the increasing of wind velocity will increase both excitation force magnitude and excitation frequency

.

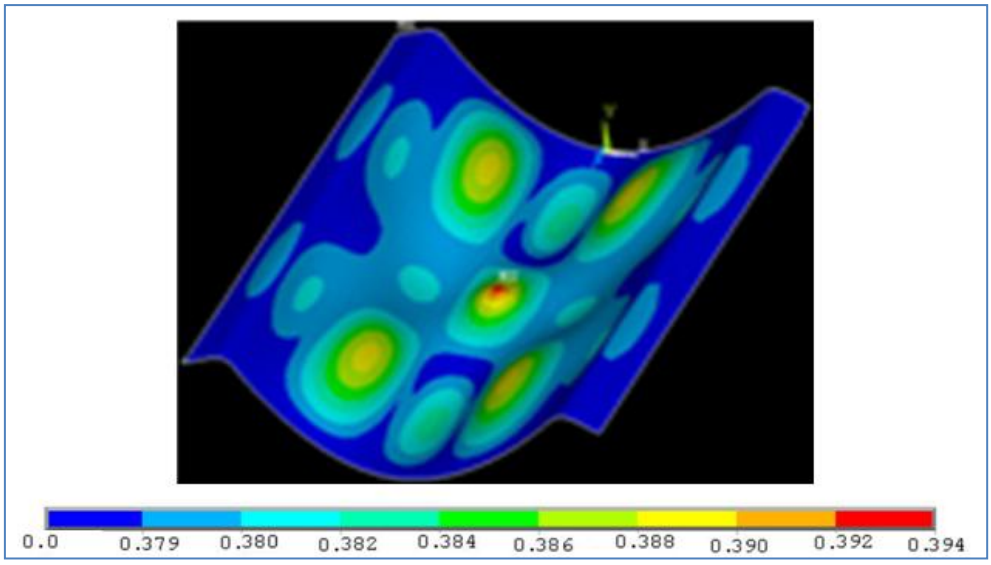

Fig. 6. Deflection of collector surface at Θ=30° and v=5m/s (dimension in mm).

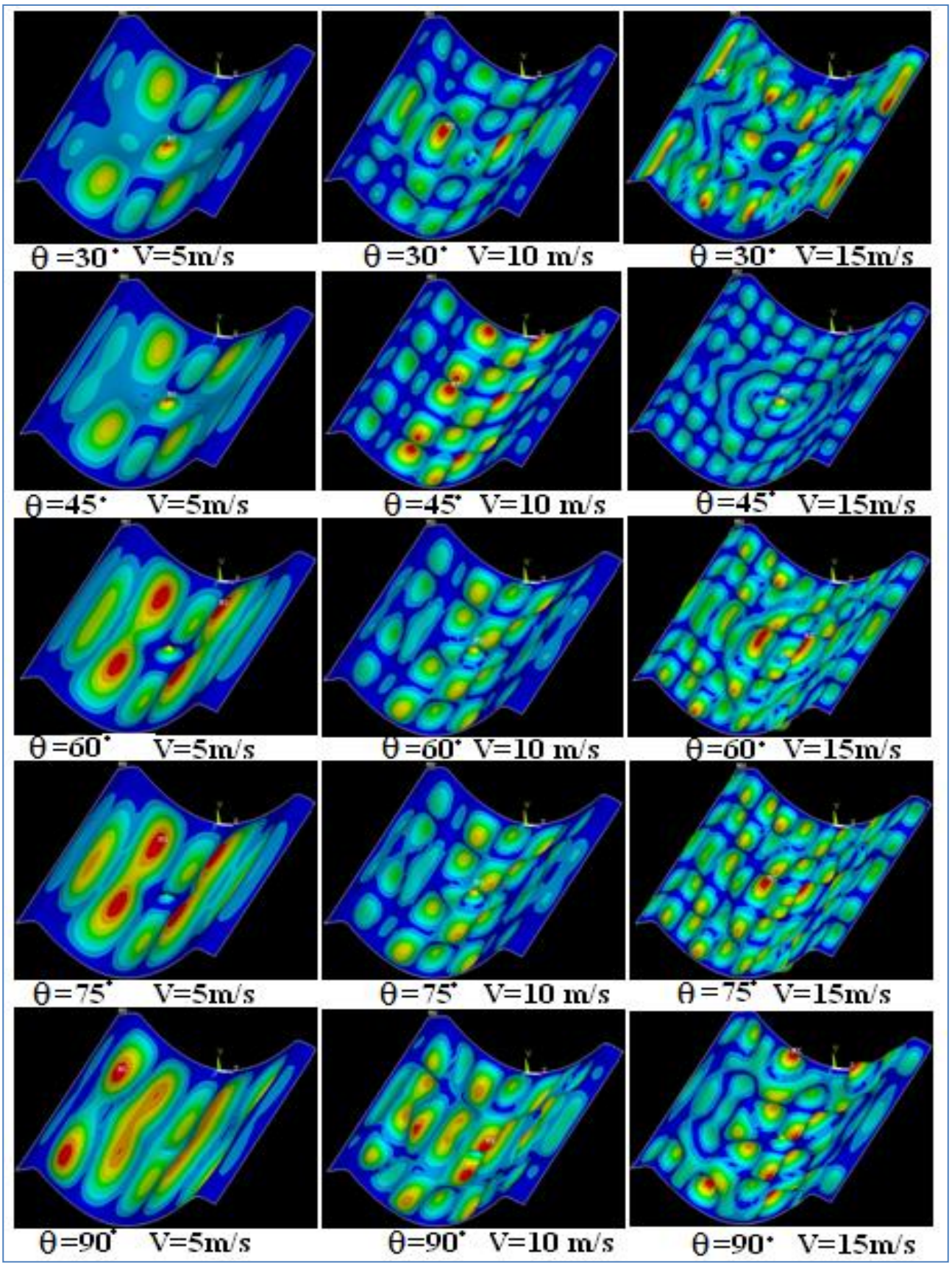

Fig.7. The deflection of trough at each wind velocity and angle of attack.

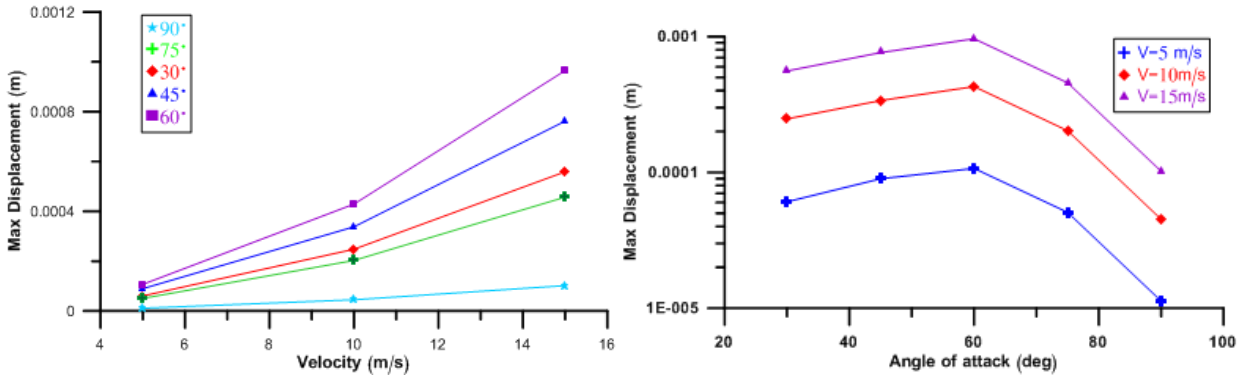

Fig. 8. The maximum deflection of trough versus angle of attack and wind velocity.

9. Solar Collector Performance Parameters

All parameters necessary for the calculation of collector performance are measured during different days of months August, September and October. These parameters are measured and collected first without vortex induced vibration and second with vortex induced vibration. Then the performance of trough for specific angle of attack and amount of solar radiation with vortex induced vibration was compared with the performance of trough for the same angle of attack and amount of solar radiation without vortex induced vibration. Table (5) lists the typical data necessary for performance analysis during the day from October month. Then the thermal efficiency of trough are calculated for both cases and compared. Figure (9) shows the thermal efficiency of solar collector for five angles of attack for period of time between 9:00 A.M. to 2:00 P.M. with and without vortex induced vibration. Many observations can be drawn from this figure. The first observation is that the thermal efficiency of solar collector has different trend with angles of attack.

For (θ =30˚ and 45˚), the thermal efficiency was noticed to be high during early hours of the day and then decreases around the mid noon and then increases after mid noon. This behavior of thermal efficiency is noticed for solar collector with and without applying vortex induced vibration. The reduction in thermal efficiency of solar collector around the mid noon can be attributed to the inertia of solar collector to transfer all solar energy to heat when the solar radiation reach to its maximum value at mid noon. The maximum value of thermal efficiency for both these angles of attack without vortex induced vibration is approximately (0.47) while the minimum value is (0.35) for (θ=30˚) and (0.33) for (θ=45˚). The applying of vortex induced vibration on solar collector leads to decreasing the value of thermal efficiency significantly. Increasing of the wind velocity leads to more decreasing in the value of thermal efficiency. The larger decreasing in thermal efficiency occurs at wind velocity (15m/s). This reduction in thermal efficiency attributed to deviation of sun light because the changes in collector profile due to wind excitation. The amount of these changes in collector profile depends on the amount of external excitation and the vibrational characteristics of the structure. It is clear that the increasing of wind velocity leads to excite the structure to vibrate in high mode as shown in figure (6) because the increasing of wind velocity leads to increase the vortex shedding frequency. High mode of vibration means more concaves in collector surface and more deviations of sun light. It is clear from figure (6) that the increasing of wind velocity leads to increase the number of concaves on collector surface for all angles of attack.

For (θ=60˚, 75˚ and 90˚) without vortex excitation, the thermal efficiency was noticed to exhibit little fluctuating around specific value along the test period. Also, the thermal efficiency of solar collector with vortex excitation is noticed to be less than that without wind velocity and has fluctuated values around specific value except that for (θ=60˚) and vortex excitation 15m/s where large reduction in thermal efficiency is appear. This reduction increases as the local time increase until reach to maximum reduction at 12:00 o'clock. This reduction can be attributed to the effect of vortex excitation because that excitation was shown to be maximum at angle of attack (θ=60˚). diffusion

Table 5,
Typical performance data of solar collector.

Time (hr)	T_{amb} (c°)	T_{in} (c°)	T_{out} (c°)	$q_S=I_d+I_b$ W/m^2	I_d W/m^2	I_b W/m^2	Q (W)	η_{sys}
9:00	33	43.1	44.3	462	77	385	504	0.425
9:30	34.3	45.2	46.5	515	80	435	546	0.407
10:00	35	48.7	50.1	571	81	490	588	0.390
10:30	35.5	54.3	55.8	629	84	545	630	0.375
11:00	36.1	60.5	62	678	85	593	630	0.345
11:30	36.7	64	65.6	728	88	640	672	0.340
12:00	37.3	68.4	70.1	775	91	684	714	0.338
12:30	37.5	72.4	73.7	701	86	615	546	0.288
1:00	37.9	77	78.3	688	85	603	546	0.294
1:30	38.5	80.2	81.6	672	82	590	588	0.323
2:00	38.9	84.3	85.7	660	79	581	588	0.328

Also, the useful heat gain is computed for each angle of attack without vortex induced vibration and with vortex induced vibration. Figure (10) shows the polynomial curveting of the results of useful heat gain without and with vortex induced vibration for two typical angles of attack (60˚ and 75˚). It is shown from this figure that the vortex induced vibration leads to remarkable decreasing in useful heat gain. This decreasing in useful heat gain increases with wind velocity at early time but become closely at after noon. Also, the presence of vortex excitation does not change the trend of the gain where the maximum value of gain is recorded at about 12:00 o'clock when the vortex excitation is applied or not.

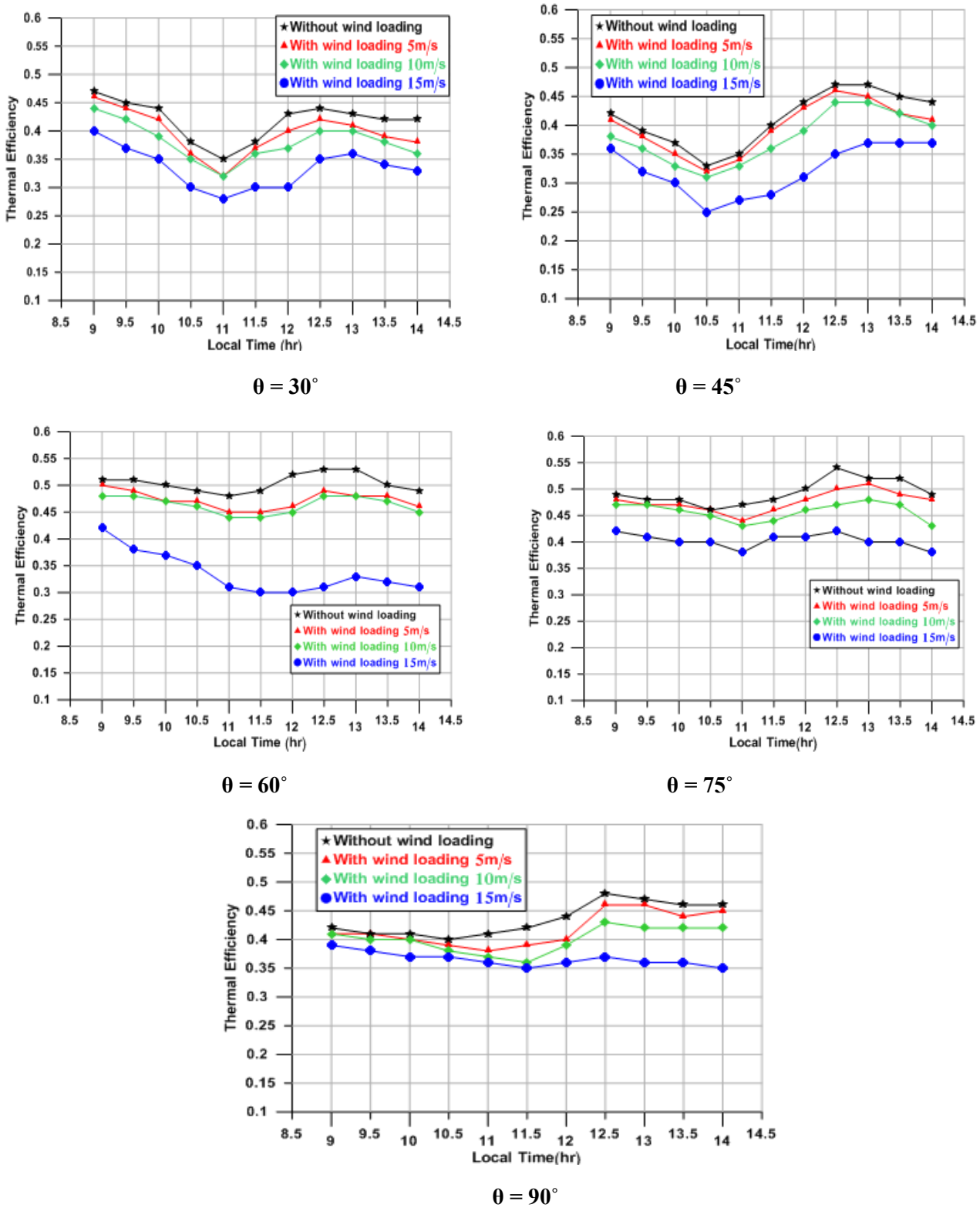

Fig. 9. Thermal efficiency of solar collector at each angle of attack with and without wind induced vibration.

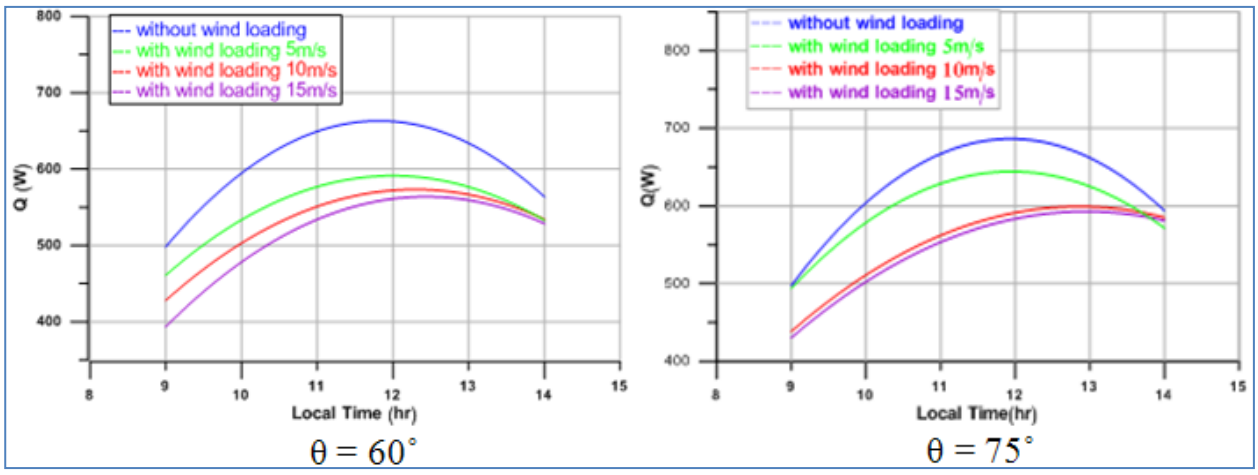

Fig. 10. Useful heat gain for two angles of attack with and without wind induced vibration.

10. Conclusions

1- The presence of vortex induced vibration leads to decreasing both thermal efficiency and useful heat gain but does not change the trend of variation with local time.
2- The increasing of wind velocity leads to more decreasing of thermal efficiency and useful heat gain.
3- The maximum decreasing of thermal efficiency with vortex excitation is noticed at angle of attack (60˚ and 75˚).
4- The excitation of the structure to vibrate at high modes of vibration will increase the degradation of the collector performance.

Notation

A	Collector aperture area [m^2]
C_L	Lift coefficient
C_w	Water specific heat [kJ/kg.K]
D	Object diameter [m]
F	Lift force [N]
F_s	Vortex shedding frequency [Hz]
m_w	Water mass flow rate [kg/s]
PTSC	Parabolic trough solar collector
Q	Heat gain [W]
I_b	Beam solar intensity [W/m^2]
I_d	Diffusion solar intensity [W/m^2]
q_s	Total intensity of solar radiation [W/m^2]
S	Strohal number
T_i	Inlet temperature [K]
T_e	Outlet temperature [K]
T_{amb}	Ambient temperature [K]
U	Wind velocity [m/s]

Greek letters

Θ	Angle of attack [degree]
P	Fluid density [kg/m^3]
η_c	Collector effeciency

11. References

[1] Eckhard, et. al, " Eurotrough design issues and prototype testing at PSA", Proceedings of Solar Forum, Washington, 2001.
[2] Yaghoubi M, Sefidbakht S, Kenary A. Performance variation of 250kW solar thermal power plant for various locations in Iran. In: Proceedings of second international conference on energy research & development, State of Kuwait, 2002. p. 765–75.
[3] Paidoussis M.P., "Fluid-Structure Interaction Vol.2: Slender Structures and Axial Flow", Elsevier Academic Press, London, 2004.
[4] Mukund R. Patel "Wind and Solar Power systems: Design, Analysis, and Operation", Taylor & Francis, second edition, 2006.
[5] Holmes JD, Banks RW, Roberts G. Drag and aerodynamic interference on microwave dish antennas and their supporting towers. J Wind Eng Ind Aerodyn 1993;50:263–9.
[6] [6]Raddu A, Axinte E. Wind forces on structures supporting solar collectors. J Wind Eng Ind Aerodyn 1989;32:93–100.
[7] L. Chevalien, J. Norton, Wind loads on solar collector panels and support structure, Aerospace Engineering Department, Texas A&M University (1979).

[8] G.A. Kopp, D. Surry, Wind loads on solar array, Wind and Structures. 5, (2002) 393-406.
[9] Alan G. Davenport, Milos Novak, "Vibration of structures induced by wind", McGraw-Hill Book Company, Inc., New York, 1966.
[10] R. K. Foran, " Vibration and flow field characteristics of a solar concentrator", M.Sc. thesis, Texas Tech University, 1984.
[11] R. D. Blevins, "Flow-induced vibration", second edition., Kreiger, Malibar, 1994.
[12] J.A. Peterka, N. Hosoya, R.C. Gee and D. Kearney," Wind Tunnel Tests of Parabolic Trough Solar Collectors" National Renewable Energy Laboratory, NREL/SR-550-32282, May 2008.
[13] Garg. H. P. and Prakash J., "Solar Energy Fundamentals and Applications", Tata McGraw-Hill Publishing Company Limited, Tenth reprint, 2008.

Appedix1: Details of Numerical Simulation Parameters

Model geometry: Parabolic trough solar collector

Boundary conditions: clumped-clumped for curved edges and free-free for straight edges.

Material: isotropic composite material with density (1455kg/m^3) and poisons ratio (0.38).

Governing equations: the equation of motion for free and forced vibration

1- free vibration $[m]\{\ddot{x}\} + [c]\{\dot{x}\} + [k]\{x\} = 0$

2- forced vibration $[m]\{\ddot{x}\} + [c]\{\dot{x}\} + [k]\{x\} = F_o sin\omega t$

where

[m] : mass matrix

$\{\ddot{x}\}$: acceleration vector

[c] : damping matrix

$\{\dot{x}\}$: velocity vector

[k]: stiffness matrix

{x}: displacement matrix.

The SHELL281 was used in current study. This element is suitable for analyzing thin to moderately-thick shell structures. The element has eight nodes with six degrees of freedom at each node: translations in the x, y, and z axes, and rotations about the x, y, and z-axes.

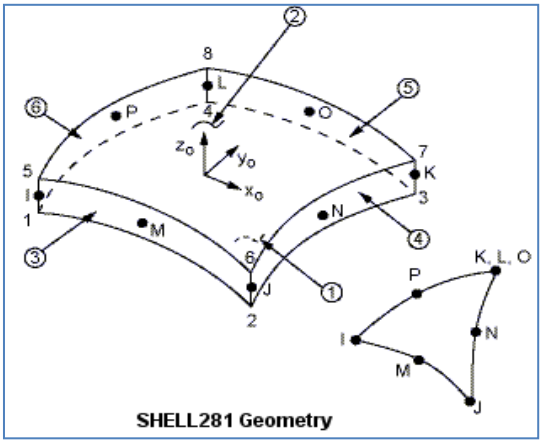

Fig. E1.1. Showing element type.

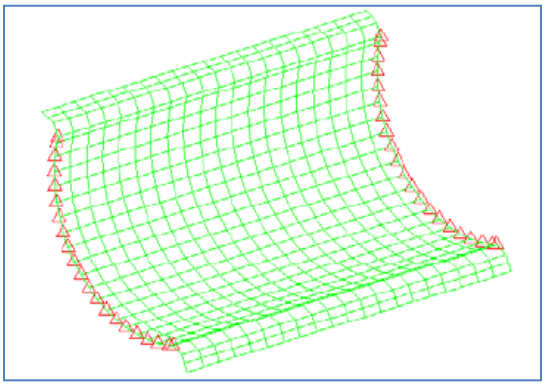

Fig. E1.2. Showing mashing model.

دراسة عملية لتأثير انبثاق الدوامات على كفاءة المجمع الشمسي

علاء الدين عبد القادر كاظم
قسم الشؤون الهندسية / جامعة بغداد
البريد الالكتروني: aldina81@yahoo.com

الخلاصة

في هذا البحث، أجريت دراسة تأثير انبثاق الدوامات على أداء المجمع الشمسي المصمم بشكل القطع المكافئ عملياً. تناولت الدراسة تأثير تذبذب الهيكل الناتج عن انبثاق الدوامات على نقصان كفاءة أداء المجمع . وتضمنت الدراسة حساب أداء المجمع باستخدام الكسب الحراري والكفاءة الحرارية . وقدمت محاكاة الإثارة الناتجة عن انبثاق الدوامات عملياً . تضمن البحث حساب الكسب الحراري والكفاءة الحرارية للمجمع الشمسي من قياسات عملية بدون تأثير انبثاق الدوامات وبوجود تأثير انبثاق الدوامات. كما وتم تصنيع انموذج من المجمع الشمسي لهذا الغرض . وتناولت الدراسة ايضا تأثير انبثاق الدوامات عند ظروف تشغيل مختلفة. ان تغيير زوايا الهجوم وسرعة الرياح تؤديان الى قيم مختلفة في معاملات الحمل الناتج عن الدوامات وكذلك تردد انبثاقها . تم ايجاد العلاقة بين الخواص الديناميكية للمجمع الشمسي وأداء المجمع الشمسي. كذلك استخدمت طريقة العناصر المحددة لدراسة المواصفات الديناميكية للمجمع الشمسي فضلا عن الجانب العملي لتقويم العلاقة بين السلوك الديناميكي للمجمع وأدائه.